Mass Spectrometric Studies of Alkali Metal Ion Binding on Thrombin-Binding Aptamer DNA

Eun Sun Hong,[a] Hye-Joo Yoon,[a] Byungjoo Kim,[b] Yong-Hyeon Yim,[b] Hun-Young So,[b] and Seung Koo Shin[a]

[a] Bio-Nanotechnology Center, Department of Chemistry, Pohang University of Science and Technology, Pohang, Korea
[b] Division of Metrology for Quality Life, Korea Research Institute of Standards and Science, Daejeon, Korea

The binding sites and consecutive binding constants of alkali metal ions, ($M^+ = Na^+$, K^+, Rb^+, and Cs^+), to thrombin-binding aptamer (TBA) DNA were studied by Fourier-transform ion cyclotron resonance spectrometry. TBA–metal complexes were produced by electrospray ionization (ESI) and the ions of interest were mass-selected for further characterization. The structural motif of TBA in an ESI solution was checked by circular dichroism. The metal-binding constants and sites were determined by the titration method and infrared multiphoton dissociation (IRMPD), respectively. The binding constant of potassium is 5–8 times greater than those of other alkali metal ions, and the potassium binding site is different from other metal binding sites. In the 1:1 TBA–metal complex, potassium is coordinated between the bottom G-quartet and two adjacent TT loops of TBA. In the 1:2 TBA–metal complex, the second potassium ion binds at the TGT loop of TBA, which is in line with the antiparallel G-quadruplex structure of TBA. On the other hand, other alkali metal ions bind at the lateral TGT loop in both 1:1 and 1:2 complexes, presumably due to the formation of ion-pair adducts. IRMPD studies of the binding sites in combination with measurements of the consecutive binding constants help elucidate the binding modes of alkali metal ions on DNA aptamer at the molecular level. (J Am Soc Mass Spectrom 2010, 21, 1245–1255) © 2010 American Society for Mass Spectrometry

A single-stranded DNA containing the 15-nucleotide sequence d(GGTTGGTGTGGTTGG) binds and inhibits thrombin, thus called thrombin-binding aptamer (TBA) [1]. The active form of TBA adopts a chair-type intramolecular G-quadruplex (G4), where the two G-tetrads are interconnected through the lateral TT and TGT loops in antiparallel conformation [2–6]. Some metal ions induce the structural transition to the G4 structure upon binding [7–10]. The binding modes of metal ions on the G4 structure are of fundamental interest in understanding their specific and/or non-specific interactions. Various methods have been applied to the studies of binding modes and structures of TBA–metal complexes. NMR experiments have shown that potassium induces the chair-type G-quadruplex formation, but sodium does not [11]. Circular dichroism (CD) and UV absorption studies have shown that potassium, strontium, and barium stabilize the G4 structure in solution [12]. Recently, electrospray ionization mass spectrometry (ESI-MS) has confirmed the unimolecular G4 structure of TBA–metal (metal = potassium, strontium and barium) complexes in the gas phase by H/D exchange [13]. Here, we studied the binding modes of alkali metal ions on TBA and determined the consecutive binding constants to unravel the specific and/or non-specific interactions between alkali metal ions and G4 TBA.

Most of the structural studies carried out in solution deal with an ensemble of dynamic structures present under ambient conditions. To more firmly establish the binding mode, we need to employ a molecular probe that is selective toward the specific ions of interest. ESI-MS offers a mass-specific means to bring the complex ions present in solution into the gas-phase [14, 15] for the studies of noncovalent ligand–nucleic acid interactions. Moreover, ESI-MS has been successfully used in validating the G4 structure of TBA [13], sequencing oligonucleotides [16, 17], and obtaining the IR spectra of G4 DNA [18]. In this report, we generated the 1:1 and 1:2 TBA–alkali metal (sodium, potassium, rubidium, and cesium) complex ions by ESI, determined the consecutive binding constants, and carried out sequencing by infrared multiphoton dissociation (IRMPD). To check the structure of TBA in ESI solvent in the presence or absence of alkali metal ions, we performed CD analysis. For the binding constant measurement [15, 19–24], we used the titration method [21, 23, 24]. The relative abundances of metal-bound and unbound

Address reprint requests to Dr. H.-J. Yoon and Dr. S. K. Shin, Department of Chemistry, Pohang University of Science and Technology, Pohang, Kyungbuk 790-784, Korea. E-mail: hjyoon@postech.ac.kr; skshin@postech.ac.kr

© 2010 American Society for Mass Spectrometry. Published by Elsevier Inc.
1044-0305/10/$32.00
doi:10.1016/j.jasms.2010.03.035

Published online April 2, 2010
Received December 14, 2009
Revised March 9, 2010
Accepted March 10, 2010

TBA in the ESI mass spectra were used to calculate the consecutive binding constants. To determine the metal binding sites, we applied IRMPD [16, 25]. As the efficient absorption of IR photons at 10.6 μm by phosphate groups induces phosphodiester backbone cleavage [26–29], the binding sites of metal ions can be directly determined from the fragmentation pattern and the fragment charge distribution. By taking both the consecutive binding constants and the binding sites into consideration, we suggest a specific interaction between alkali metal ions and G4 TBA formed in ESI solvent.

Experimental

Sample Preparation

TBA purified by C_{18}-column was purchased from Bioneer (Daejeon, Korea) and used without further purification. Sodium chloride (99.999%), potassium chloride (99.999%), rubidium chloride (99+%), cesium chloride (99.999+%), and other chemicals were purchased from Sigma-Aldrich (St. Louis, MO, USA). A stock solution of TBA (100 μM) was prepared by dissolving dry powder in ammonium acetate buffer (150 mM, pH 7.0), immersing a sample tube containing TBA in a 95 °C oil bath for 10 min, and then cooling it to room temperature. ESI samples were prepared by diluting the stock solution to a 1:10 ratio in a 1:1 (vol/vol) water/isopropanol solution. Both TBA and alkali metal chloride stock solutions were mixed in water and then mixed with isopropanol for ESI. The final solute concentration was 10 μM for TBA, 100 μM for metal chloride, and 15 mM for ammonium acetate.

Mass Spectrometry

A 12-Tesla Fourier-transform ion cyclotron resonance (FT-ICR) spectrometer (Varian, Lake Forrest, CA, USA) was used for both titration and IRMPD experiments. This instrument was equipped with a Nanomate-100 chip (Advion, Ithaca, NY, USA) for ESI and a Synrad 48–2 CO_2 laser (Mukilteo, WA, USA) for IRMPD as previously described in detail [30]. The ESI mass spectra were taken in negative mode under Nanomate conditions of 1.6-kV applied voltage and 0.2-p.s.i. nitrogen pressure. The ion of interest was mass-selected by ejecting all unwanted ions using stored waveform inverse Fourier transform (SWIFT). Remaining ions in the ICR cell were irradiated with 10.6 μm CO_2 laser for 300 ms by increasing the laser fluence from 0.56 to 1.25 J cm^{-2}. The IR laser beam passed through a BaF_2 vacuum window and crossed a cylindrical ICR cell once. ICR transients were acquired in broadband mode with 1.024 M data points at the sampling rate of 2 MHz in the mass range of m/z = 190–2500 Th. The time-domain transient signal was processed with a Blackman window.

Binding Constant Measurement

Sample solutions containing TBA (10 μM) mixed with metal chlorides (10–400 μM) were prepared and the ESI mass spectra of TBA were taken in negative mode as a function of metal ion concentration. Relative abundances of TBA, 1:1 and 1:2 TBA–metal (TBA–M^+) complex ions were used to derive the binding constants. The metal ion forms complexes with TBA by consecutive equilibria as given in eqs 1 and 2.

$$\mathrm{TBA} + \mathrm{M}^+ \rightleftarrows (\mathrm{TBA} + \mathrm{M}^+);\ K_1 = \frac{[\mathrm{TBA} + \mathrm{M}^+]}{[\mathrm{TBA}][\mathrm{M}^+]_f}, \quad (1)$$

$$(\mathrm{TBA} + \mathrm{M}^+) + \mathrm{M}^+ \rightleftarrows (\mathrm{TBA} + 2\mathrm{M}^+);\ K_2 = \frac{[\mathrm{TBA} + 2\mathrm{M}^+]}{[\mathrm{TBA} + \mathrm{M}^+][\mathrm{M}^+]_f}, \quad (2)$$

where K_1 and K_2 are the equilibrium constants for the first and second alkali metal binding, respectively. [TBA], [TBA + M^+], and [TBA + 2M^+] represent the concentration of TBA, (TBA + M^+), and (TBA + 2M^+) ions, respectively. $[M^+]_f$ is the concentration of free metal ion, which is the difference between the initial concentration $[M^+]_0$ and the concentration of complexed metal ions $[M^+]_c$. [TBA + $n$$M^+$] ($n$ = 0–2) is calculated from the intensities of TBA, (TBA + M^+) and (TBA + 2M^+) ions in the mass spectra, as presented in eq 3.

$$(\mathrm{TBA} + n\mathrm{M}^+) = [\mathrm{TBA}]_0 \times \frac{\mathrm{I}(\mathrm{TBA} + n\mathrm{M}^+)}{\sum \mathrm{I}(\mathrm{TBA}) + \sum \mathrm{I}(\mathrm{TBA} + \mathrm{M}^+) + \sum \mathrm{I}(\mathrm{TBA} + 2\mathrm{M}^+)}, \quad (3)$$

where $[TBA]_0$ is the initial concentration of TBA, I(TBA), I(TBA + M^+), and I(TBA + 2M^+) are the intensity of TBA, (TBA + M^+), and (TBA + 2M^+) ions, respectively, and the summation on the denominator is over all possible charge states. Likewise, $[M^+]_c$ is calculated from the fraction of the metal-containing complex ions, as expressed in eq 4, and $[M^+]_f$ is derived therefrom.

$$[\mathrm{M}^+]_c = [\mathrm{TBA}]_0 \times \frac{\sum \mathrm{I}(\mathrm{TBA} + \mathrm{M}^+) + \sum 2 \cdot \mathrm{I}(\mathrm{TBA} + 2\mathrm{M}^+)}{\sum \mathrm{I}(\mathrm{TBA}) + \sum \mathrm{I}(\mathrm{TBA} + \mathrm{M}^+) + \sum \mathrm{I}(\mathrm{TBA} + 2\mathrm{M}^+)}, \quad (4)$$

$$[M^+]_f = [M^+]_0 - [M^+]_c. \quad (5)$$

Eqs 1 and 2 are rearranged to eqs 6 and 7 as a function of $[M^+]_f$.

$$\frac{[TBA + M^+]}{[TBA]} = K_1[M^+]_f, \quad (6)$$

$$\frac{[TBA + 2M^+]}{[TBA + M^+]} = K_2[M^+]_f. \quad (7)$$

Both the $[TBA + M^+]/[TBA]$ and $[TBA + 2M^+]/[TBA + M^+]$ ratios vary linearly with $[M^+]_f$ and the slope represents the equilibrium constants K_1 and K_2, respectively.

Circular Dichroism l(CD)

The CD spectra were recorded in the 200–340 nm wavelength range at a rate of 100 nm min^{-1} with a JASCO J-810 spectropolarimeter (Easton, MD, USA). A 1.0-cm path quartz cuvette was used to take the CD spectra while flushing a sample chamber with dry nitrogen. The CD spectra were taken in water as well as in ESI solvent. The solute concentration was 3 μM for TBA and 100 μM for alkali metal chloride.

Results and Discussion

ESI Mass and CD Spectra of TBA

The ESI mass spectra of TBA in the absence and presence of alkali metal ions are shown in Figure 1. TBA and TBA–M^+ complex ions (M^+ = Na^+, K^+, Rb^+, and Cs^+) were observed in 3−, 4−, and 5− charge states. No TBA–ammonium complex ions were detected. Of the three charge states, the most abundant 4− charge state was further characterized by IRMPD. When ions present in solution are transferred into the gas phase by ESI [14, 15], both the ionization efficiency and response factor may vary if the metal binding changes the structure of TBA in solution [15, 19–24]. Any changes in ionization efficiency and response factor should appear in charge-state distributions of TBA and TBA–M^+ complex ions [20, 24]. The relative abundances of TBA and TBA–M^+ complex ions are plotted in Figure 1f as a function of charge state. The charge-state distributions are almost identical, regardless of the presence or absence of alkali metal ions, indicating that the metal binding to TBA hardly alters the structure of TBA in ESI solvent.

To further examine the structure of TBA in solution, we obtained the CD spectra in 1:1 water/isopropanol in the absence and presence of alkali metal chloride and ammonium acetate (see Supplementary Material, Figure S1 which can be found in the electronic version of this article). In water, only TBA–potassium and TBA–ammonium mixtures show the characteristic feature of antiparallel G4 structure, a positive band at 295 nm and a negative band at 265 nm [12]. Other alkali metal ions do not show the G4 feature in water. On the other hand, all samples, whether or not the metal is present, display spectral characteristic of antiparallel G4 structures in water/isopropanol with/without ammonium acetate. Apparently, isopropanol induces the formation of G4-TBA [31, 32], independent of the presence or absence of potassium or ammonium ion. In ESI solvent containing ammonium acetate, potassium further stabilizes G4-

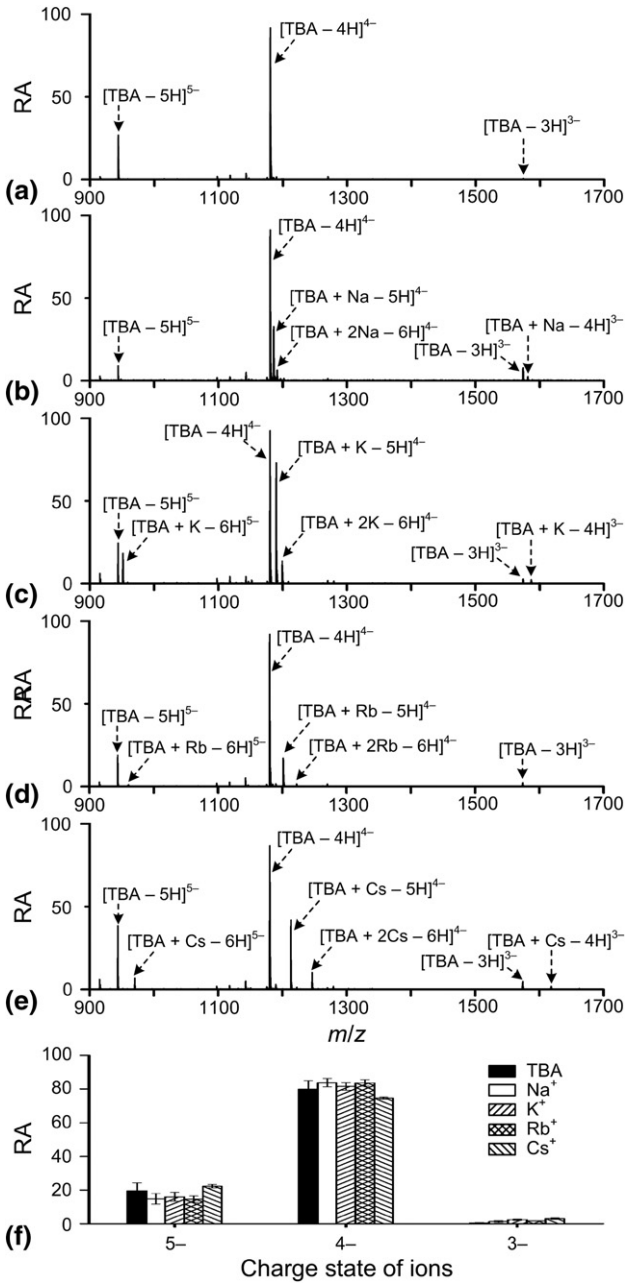

Figure 1. ESI mass spectra of (**a**) TBA (10 μM), (**b**) TBA (10 μM) plus sodium chloride (100 μM), (**c**) potassium chloride (100 μM), (**d**) rubidium chloride (100 μM), (**e**) cesium chloride (100 μM), and (**f**) relative abundances of ions as a function of charge state.

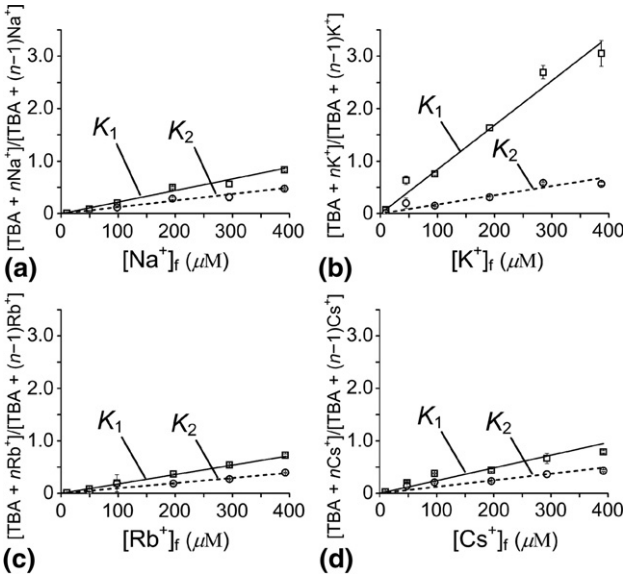

Figure 2. Plots of $[TBA + nM^+]/[TBA + (n–1)M^+]$ as a function of (**a**) $[Na^+]_f$, (**b**) $[K^+]_f$, (**c**) $[Rb^+]_f$, and (**d**) $[Cs^+]_f$. $[M^+]_f$ is the concentration of free metal ion. The ratio is derived from the relative abundances of TBA, 1:1 and 1:2 TBA–metal complex ions in the ESI mass spectra.

TBA but other metals hardly change the CD spectra of TBA, indicating a difference in binding mode between potassium and other alkali metals.

Because the metal binding to TBA does not change the structure of TBA in ESI solvent [33, 34] and the effects of metal binding on the ionization efficiency and response factors are identical for all TBA and TBA–M^+ complexes, we use the stoichiometry and relative abundances of TBA and TBA–M^+ complex ions in the ESI mass spectra to determine the metal-binding constants.

Determination of Binding Constants in TBA–Alkali Metal Ion Complexes

The $[TBA + nM^+]/[TBA + (n–1)M^+]$ (n = 1–2) ratios are shown in Figure 2 as a function of $[M^+]_f$. The first and second binding constants K_1 and K_2 are derived from the slopes corresponding to n = 1 and 2, respectively, and listed in Table 1. K_1 of 8.4 × 10^3 M^{-1} for potassium is 4–5 times greater than K_1 for other alkali metals in the range of (1.8–2.4) × 10^3 M^{-1}. Interestingly, K_2 of 1.8 × 10^3 M^{-1} for potassium is comparable to K_1 for other metals. Sodium, rubidium, and cesium exhibit similar values of K_2 in the range of (1.0–1.2) × 10^3 M^{-1}. The product of K_1 and K_2 for potassium is 5–8 times greater than the K_1K_2 values for other metals. In comparison, fluorescence spectroscopy has shown that the binding constant of potassium (K_a = 13 × 10^6 M^{-1}) is 24 times greater than that of sodium (K_a = 0.55 × 10^6 M^{-1}) in 10 mM Tris–HCl buffer [35]. The binding constant K_a obtained in solution is inherently different from the consecutive binding constants K_1 and K_2 determined by mass spectrometry because fluorescence spectroscopy does not distinguish the structures of 1:1 and 1:2 TBA–metal complexes in solution. Although direct comparison cannot be made between the two different measurements, sodium appears to bind more strongly to TBA in ESI solvent than to TBA in Tris-HCl buffer. This discrepancy is attributed to dissimilar structures of TBA in two different solvent systems. In ESI solvent, our CD results show that TBA always folds into the antiparallel G4 structure (see Figure S1). In Tris-HCl buffer, however, CD results by Tsumoto and coworkers have shown that potassium induces the formation of G4-TBA but sodium does not [36]. Similarly to CD results, NMR and molecular dynamics (MD) studies have also shown that the G4 structure of TBA is induced by potassium in Tris buffer (20 mM Tris, 140 mM NaCl, pH 7.0) but not by sodium [37]. Our CD and MS data suggest that sodium binds more tightly to G4 than other structures of TBA available in the Tris-HCl buffer.

Meanwhile, the dissociation constant (K_d) of 5000 nM has been reported for the TBA–potassium complex [23], which is 24 times smaller than K_1^{-1} of 119 μM but 76 times greater than $(K_1K_2)^{-1}$ of 66 nM. This discrepancy may be due to the dissimilar solvent system used for ESI and the effect of pH at equilibrium [38]. In the present experiment, the 1:1 water/isopropanol solvent system was used for ESI without any pH adjustment. In this solvent system, the 4– charge state ion appears predominantly by either turbospray or nanospray ionization using a hybrid quadrupole time-of-flight mass spectrometer (QSTAR-Pulsar i; Applied Biosystems, Concord, Canada). In comparison, the other experiment was carried out in water containing 25% methanol and

Table 1. Binding constants of TBA–M^+ complexes (M^+ = Na^+, K^+, Rb^+, and Cs^+)

	Binding constant[a]			
Metal	K_1 (10^3 M^{-1})	K_2 (10^3 M^{-1})	K_1K_2(10^6 M^{-2})	K_a (10^6 M^{-1}) in solution[b,c]
Na^+	2.2 ± 0.05	1.2 ± 0.04	2.6 ± 0.11	0.55 ± 0.03
K^+	8.4 ± 0.16	1.8 ± 0.04	15.1 ± 0.44	13 ± 1
Rb^+	1.8 ± 0.02	1.0 ± 0.02	1.8 ± 0.04	
Cs^+	2.4 ± 0.05	1.2 ± 0.04	2.9 ± 0.11	

[a]An error is from the least-squares fit.

[b]$K_a = \frac{[TBA+M^+]+[TBA+2M^+]}{[TBA]_f[M^+]_f} = K_1(1 + K_2[M^+]_f)$.

[c]The binding constants in solution are taken from reference [35].

0.50% NH_4OH (vol/vol) using an ion-trap mass spectrometer (LCQ Classic; ThermoFinnigan, San Jose, CA, USA).

IRMPD Spectra of [TBA – 4H]$^{4-}$

The IRMPD mass spectra of $[TBA - 4H]^{4-}$ obtained at the laser fluence of 0.90 J cm^{-2} are shown in Figure 3a and the fragmentation patterns as well as the charge and intensity distributions of fragment ions are presented in Figure 3b. The nomenclature is taken from McLuckey et al. [39]. Four possible sites of cleavage along the nth phosphodiester backbone in $(n + m)$ base DNA result in a_n–d_n fragments containing 5′-ends and w_m–z_m fragments containing 3′-ends. The efficient absorption of IR photons at 10.6 μm by phosphate groups induces cleavage at the phosphodiester backbone [25–29]. $[TBA - 4H]^{4-}$ yields $[a_n - GH]$ (n = 2, 4–6, 8, 10, 11) and w_m (m = 1, 4, 5, 7, 9, 10, 13, 14) ions. The charge distribution of fragment ions indicates that four negatively-charged phosphate groups are located at the G^1–G^2, T^4–G^5 or G^5–G^6, G^{10}–G^{11} or G^{11}–T^{12}, and G^{14}–G^{15} mid points. Both the $[a_2 - GH]^-$ and $w_{14}{}^{4-}$ ions provide evidence for the negatively-charged phosphate group at the G^1–G^2 mid point and the $w_1{}^-$ ion for that at the G^{14}–G^{15} mid point. Other alternative locations of the phosphate anions (marked grey) are assigned from the $[a_5 - GH]$ and w_4 ions having both 1− and 2− charge-states as well as $[a_6 - GH]^{2-}$ and $w_5{}^{2-}$ ions. As a result, $[TBA - 4H]^{4-}$ takes charges at both ends as well as 3–4 bases away from each terminal charge.

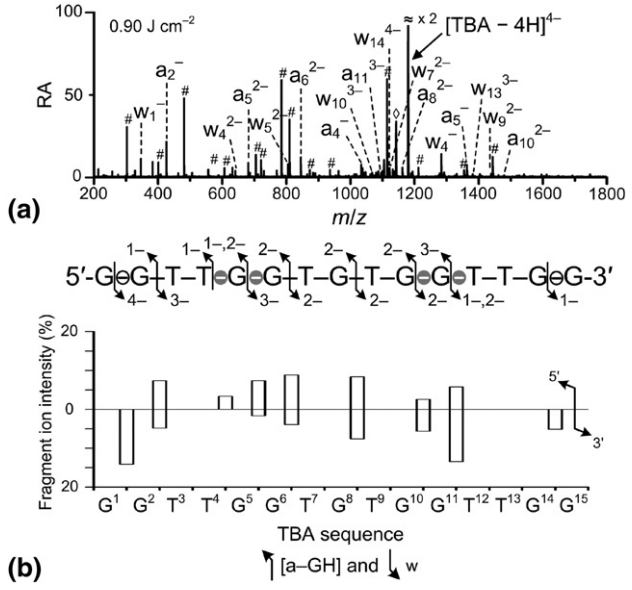

Figure 3. (**a**) IRMPD spectra of $[TBA - 4H]^{4-}$ at 0.90 J cm^{-2}. Open diamond (◇) represents loss of guanine from the parent ion and sharp symbol (#) refers to internal ions; (**b**) fragmentation pattern, charge distribution, and fragment ion intensity distribution from IRMPD of $[TBA - 4H]^{4-}$. The charge state is given next to arrowhead. The location of phosphate anion is marked by minus sign in circle. Open circle denotes the fixed location and grey circle refers to other alternatives.

Power Dependence of IRMPD

The IRMPD spectra of the TBA–sodium and TBA–potassium complex ions are obtained at three different laser fluence of 0.56, 0.90, and 1.25 J cm^{-2}, as displayed in Figures 4 and 5, respectively. At 0.56 J cm^{-2}, loss of neutral bases occurs sequentially without backbone cleavage. Moreover, the abundance of the parent ion relative to the total ions is 60%–64% for TBA–sodium complexes and 37%–60% for TBA–potassium complexes. The relative abundance of internal ions is 14%–20% for both metal complexes. Backbone cleavage takes place at higher IR fluence [25, 29]. However, as the laser fluence increases to 1.25 J cm^{-2}, the relative abundance of the parent ion decreases to 0.5%–14%, but that of internal ions increases to 37%–80%. Although the yield of primary fragmentation increases at high laser fluence, that of secondary fragmentation also increases concomitantly. For example, the longest primary fragment ions, such as w_{14} and $[a_{14} - GH]$, further dissociate to shorter fragments, such as w_1, $[a_2 - GH]$, and other internal ions. For the determination of the metal-binding sites in TBA–metal complexes, therefore, we carried out IRMPD experiments at the intermediate laser fluence, 0.90 J cm^{-2}.

Sodium-Binding Sites of TBA–nNa$^+$ Complexes (n = 1–2)

The IRMPD mass spectra of 1:1 and 1:2 TBA–sodium complexes shown in Figures 4a and b, respectively, provide the fragmentation patterns as well as the charge and intensity distributions of fragment ions, as presented in Figures 4c and d, respectively. Since IR absorption imparts no collisional impact on the ion, we expect that the cation is sequestered by the nearby phosphate anion during fragmentation. Thus the binding site of metal ion can be determined from the combination of fragmentation pattern and fragment charge distribution.

$[TBA + Na^+ - 5H]^{4-}$ yields a series of $[a - GH]$ and w ions indicating G^8–T^9 cleavage at the central TGT region. The fragment charge distribution indicates that the five negatively-charged phosphates are located at the G^1–G^2, T^4–G^5 or G^5–G^6, T^7–G^8 or G^8–T^9, G^{10}–G^{11} or G^{11}–T^{12}, and G^{14}–G^{15} mid points. The locations of negatively-charged phosphates are identical to those for the $[TBA - 4H]^{4-}$ ion except for the T^7–G^8–T^9 region. Sodium is present in $[a_n - GH]$ (n = 8, 10, 11) and w_m (m = 7, 9, 14) ions, but absent in $[a_n - GH]$ (n = 2, 4–6) and w_m (m = 1, 4, 5) ions, bracketing the location of sodium between T^7 and T^9. This T^7–G^8–T^9 region is where both the negative-charged phosphate group and sodium are found together. Since the cation is sequestered by the nearby phosphate anion during fragmentation, the positional overlap between phosphate and sodium identifies the T^7–G^8 or G^8–T^9 mid point as the binding site of sodium. The two complementary ions, $[a_8 - GH + Na]^{2-}$ and $w_7{}^{2-}$, and the other two comple-

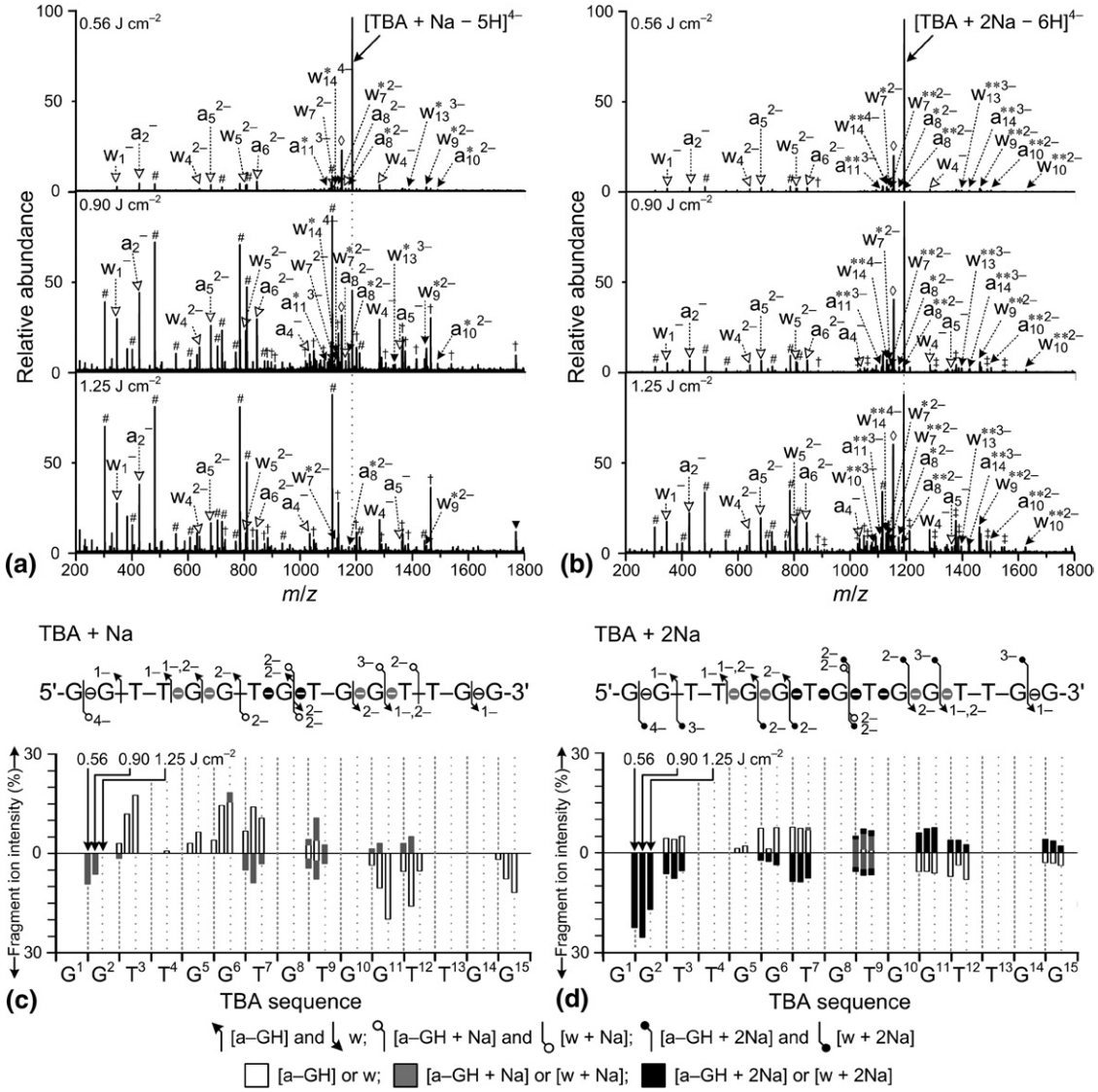

Figure 4. IRMPD spectra of (**a**) $[TBA + Na^+ - 5H]^{4-}$ and (**b**) $[TBA + 2Na^+ - 6H]^{4-}$ obtained by varying IR fluence from 0.56, 0.90, to 1.25 J cm^{-2}. Asterisk (*) indicates fragment ions containing metal ion and the number of asterisks equals to the number of metal ions bound to fragment ions. Dagger (†) and double dagger (‡) refer to internal ions with one and two metal ions, respectively; fragmentation pattern, charge distribution and fragment ion intensity distribution from IRMPD of (**c**) $[TBA + Na^+ - 5H]^{4-}$ and (**d**) $[TBA + 2Na^+ - 6H]^{4-}$. Black circle represents the possible metal-binding site.

mentary ions, $[a_8 - GH]^{2-}$ and $[w_7 + Na]^{2-}$, provide evidence of the T^7–G^8 and G^8–T^9 mid points for the sodium-binding site, respectively. Since only the metal-containing fragments can provide information on the metal-binding sites, their relative abundances are used to calculate the occupancy of metal ion at each binding site. The occupancies of 0.55 at T^7–G^8 and 0.45 at G^8–T^7 are determined from the relative intensities of the $[a_8 - GH + Na]^{2-}$ and $[w_7 + Na]^{2-}$ ions (see Supplementary Material).

With two sodiums, $[TBA + 2Na^+ - 6H]^{4-}$ yields a fragmentation pattern almost identical to that of $[TBA + Na^+ - 5H]^{4-}$. The six phosphate anions are located at the G^1–G^2, T^4–G^5 or G^5–G^6, G^6–T^7 and/or T^7–G^8, G^8–T^9 and/or T^9–G^{10}, G^{10}–G^{11} or G^{11}–T^{12}, and G^{14}–G^{15} mid points. Two sodium ions are found in $[a_n - GH]$ (n = 8, 10, 11) and w_m (m = 7, 9, 10, 13, 14) ions, only one sodium in $[a_n - GH]$ (n = 8) and w_m (m = 7) ions, and no sodium in $[a_n - GH]$ (n = 2, 4–6) and w_m (m = 1, 4, 5) ions. Thus, the location of two sodium ions is bracketed between G^6 and G^{10}. The occupancy of sodium is not determined because of the absence of $[a_n - GH]$ (n = 7, 9) and w_m (m = 6, 8) ions containing sodium. Nonetheless, the fragmentation pattern indicates that the two sodium ions are bound at the G^6TGTG^{10} loop region of TBA. The two complementary ions, $[a_8 - GH + nNa]^{2-}$ and $[w_7 + nNa]^{2-}$ (n = 0–2), provide evidence of the G^6TGTG^{10} region for the sodium binding sites. Apparently, the two sodium ions

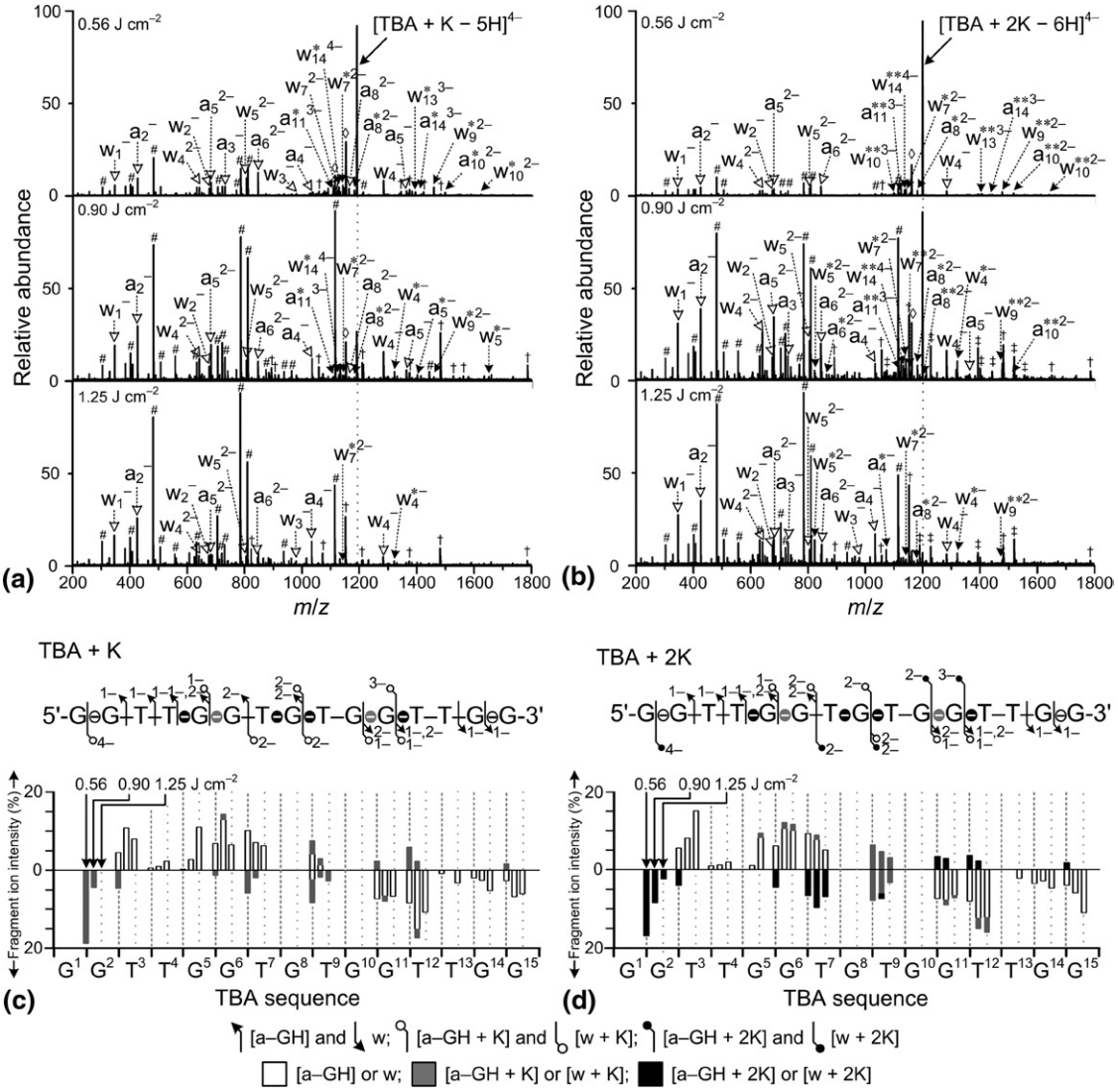

Figure 5. IRMPD spectra of (**a**) $[TBA + K^+ - 5H]^{4-}$ and (**b**) $[TBA + 2K^+ - 6H]^{4-}$ at 0.56, 0.90, and 1.25 J cm^{-2}; fragmentation pattern, charge distribution and fragment ion intensity distribution from IRMPD of (**c**) $[TBA + K^+ - 5H]^{4-}$ and (**d**) $[TBA + 2K^+ - 6H]^{4-}$.

form adducts with phosphate anions in the G^6TGTG^{10} loop region of TBA.

Potassium-Binding Sites of TBA–nK^+ Complexes (n = 1–2)

The IRMPD mass spectra of 1:1 and 1:2 TBA–potassium complexes are shown in Figures 5a and b, respectively, and their fragmentation patterns and charge and intensity distributions of fragment ions are presented in Figures 5c and d, respectively. $[TBA + K^+ - 5H]^{4-}$ results in a fragmentation pattern similar to that of $[TBA + Na^+ - 5H]^{4-}$ but with a different metal ion distribution. Potassium appears in $[a_n - GH]$ (n = 5, 8, 11) and w_m (m = 4, 5, 7, 9, 14) ions, suggesting the location of potassium between T^4 and T^{12}. The five phosphate anions are located at the same positions as $[TBA + Na^+ - 5H]^{4-}$. Overlapping positions of phosphate and potassium indicate three possible binding sites for potassium, T^4–G^5, T^7–G^8 or G^8–T^9, and G^{11}–T^{12} mid points, as evidently shown by $[a_5 - GH + K]^-$, $[a_8 - GH + K]^{2-}$, $[w_7 + K]^{2-}$, and $[w_4 + K]^-$ ions, respectively. The occupancy of potassium is estimated to be 0.425 at T^4–G^5, 0.075 at T^7–G^8–T^9, and 0.5 at G^{11}–T^{12} (see Supplementary Material).

With two potassium ions, $[TBA + 2K^+ - 6H]^{4-}$ yields a fragmentation pattern almost identical to that of $[TBA + K^+ - 5H]^{4-}$. The six phosphate anions are located at the G^1–G^2, T^4–G^5 and/or G^5–G^6, T^7–G^8 or G^8–T^9, G^{10}–G^{11} and/or G^{11}–T^{12}, and G^{14}–G^{15} mid points. Two potassium ions are found in $[a_n - GH]$ (n = 10, 11) and w_m (m = 7, 9, 14) ions, only one potassium in $[a_n - GH]$ (n = 5, 6, 8) and w_m (m = 4, 5, 7) ions, and no potassium in $[a_n - GH]$ (n = 2–6) and w_m (m = 1, 2, 4, 5) ions. Thus, the location of potassium is bracketed between T^4 and T^{12}. Overlap of phosphates with potassium identifies

two separate binding sites for potassium, the T^4–G^5 or G^{11}–T^{12} mid point for one and the T^7–G^8–T^9 region for another. The evidence for another potassium occupying at the T^7–G^8–T^9 region comes from the difference in the number of potassium between $[a_8 - GH + K]^{2-}$ and $[a_{10} - GH + 2K]^{2-}$ as well as between $[w_7 + K]^{2-}$ and $[w_9 + 2K]^{2-}$. The occupancy of potassium is estimated to be 0.42 at T^4–G^5 and 0.58 at G^{11}–T^{12}, and 0.45 at T^7–G^8 and 0.55 at G^8–T^9 (see Supplementary Material).

Potassium binds at the T^4–G^5, T^7–G^8 or G^8–T^9, and G^{11}–T^{12} mid points in the 1:1 complex. However, the occupancy of potassium indicates that the probability of potassium coordination by T^4, G^5, G^{11}, and T^{12} is ~12 times higher than that of adduct formation at the TGT region. In the case of 1:2 TBA–potassium complex, one potassium binds at the T^4–G^5 or G^{11}–T^{12} mid point and the second one at the T^7–G^8 or G^8–T^9 mid point, indicating that one potassium is coordinated between the bottom G-tetrad and two TT loops and another one binds at the T^7GT^9 region. This is consistent with the G4 structure determined by NMR and MD studies [11, 38].

Rubidium- and Cesium-Binding Sites of TBA–nM^+ Complexes (n = 1–2, M^+ = Rb^+ and Cs^+)

The IRMPD spectra, fragmentation patterns and charge distributions of the 1:1 and 1:2 TBA–rubidium and TBA–cesium complex ions are presented in Figure 6. The fragmentation patterns and the charge distributions of TBA complexes with rubidium and cesium are almost identical to those of the TBA–Na^+ complexes.

In the 1:1 complexes, the charge distribution of fragment ions indicates that the five negatively-charged phosphates are located at the G^1–G^2, T^4–G^5 or G^5–G^6, T^7–G^8 or G^8–T^9, G^{10}–G^{11} or G^{11}–T^{12}, and G^{14}–G^{15} mid points. Rubidium is present in $[a_n - GH]$ (n = 8, 10, 11, 14) and w_m (m = 7, 9, 10, 13, 14) ions but absent in $[a_n - GH]$ (n = 2, 3, 5, 6, 8) and w_m (m = 1, 2, 4, 5, 7) ions, suggesting the presence of rubidium between T^7 and T^9. Cesium is present in $[a_n - GH]$ (n = 8, 11) and w_m (m = 7, 9, 10, 13, 14) ions but absent in $[a_n - GH]$ (n = 2, 3, 5, 6, 8) and w_m (m = 1, 4, 5, 7) ions. Thus, the location of cesium is also bracketed between T^7 and T^9. The spatial overlap between phosphates and metal ions identifies the T^7–G^8 and G^8–T^9 mid points as the binding site for both rubidium and cesium. The occupancy of rubidium at the T^7–G^8 and G^8–T^9 mid points is estimated to be 0.49 and 0.51, respectively and that of cesium is 0.39 and 0.61, respectively (see Supplementary Material).

In the 1:2 complexes, the charge distributions of fragment ions are identical to that of $[TBA + 2Na^+ - 6H]^{4-}$. With two rubidium ions, $[TBA + 2Rb^+ - 6H]^{4-}$ yields the fragmentation pattern not much different from that of $[TBA + Rb^+ - 5H]^{4-}$. Two rubidium ions are found in $[a_n - GH]$ (n = 10, 11) and w_m (m = 9, 14) ions, only one rubidium in $[a_n - GH]$ (n = 8) and w_m (m = 7) ions, and no rubidium in $[a_n - GH]$ (n = 2–6) and w_m (m = 1–5) ions. Also, $[TBA + 2Cs^+ - 6H]^{4-}$ dissociates to $[a_n - GH]$ (n = 10, 11) and w_m (m = 9, 13, 14) ions with two cesiums, $[a_n - GH]$ (n = 8) and w_m (m = 7) ions with only one cesium, and $[a_n - GH]$ (n = 2, 3, 5, 6) and w_m (m = 1–5) ions without cesium. These results indicate that two rubidium or two cesium ions are located in the same region bracketed between G^6 and G^{10}. Evidently, both rubidium and cesium ions form adducts with phosphate anions in the G^6TGTG^{10} loop region of TBA.

Structures of TBA–M^+ Complexes (M^+ = Na^+, K^+, Rb^+, and Cs^+)

The fragmentation pattern and charge distribution of sodium, rubidium, and cesium are almost identical to one another, but those of potassium are not. Based on the fragmentation patterns and occupancies, the structures of TBA–M^+ complexes are proposed in Scheme **1**. In the case of the TBA–K^+ complexes, the first potassium ion is coordinated between the bottom G-quartet and two adjacent TT loops and the second one is bound at the TGT loop of TBA. This structure is consistent with that reported by NMR and MD simulations [11, 38]. On the other hand, other alkali metal ions, Na^+, Rb^+, and Cs^+, bind at the G^6TGTG^{10} loop region of TBA, presumably by forming adducts with negatively charged phosphates in that loop region. Notably, the fragment charge distributions suggest that four phosphate groups in the G^2–T^3–T^4 and T^{12}–T^{13}–G^{14} regions always carry protons in the presence or absence of alkali metal ions, even though all other phosphate groups can take negative charges. This indicates that the four phosphate groups in two TT loops are not easily ionized by solvent and may be protected by thymine through intramolecular hydrogen bonding. This interpretation is in line with an NMR finding that the TT loops are not easily accessible by the solvent [40].

Although the metal-binding sites for Na^+, Rb^+, and Cs^+ do not provide information about the structure of TBA, the G-quadruplex structure of TBA is adopted in Scheme **1** for the following reasons. Firstly, the charge-state distribution in the ESI mass spectra of TBA is identical regardless of the presence or absence of alkali metal ions. Secondly, the CD spectra of TBA in ESI solvent display the characteristic feature of the G4 structure in the presence or absence of any alkali metal ion; even though only potassium induces such a feature in water (see Figure S1). Apparently, the ESI solvent having a much lower dielectric constant than water induces the formation of the G4 structure [31, 32]. Lastly, the second potassium binding constant is almost identical to the first alkali metal binding constants for Na^+, Rb^+, and Cs^+, indicating the structure of TBA to which alkali metal ions bind is similar to the G-quadruplex structure stabilized by potassium.

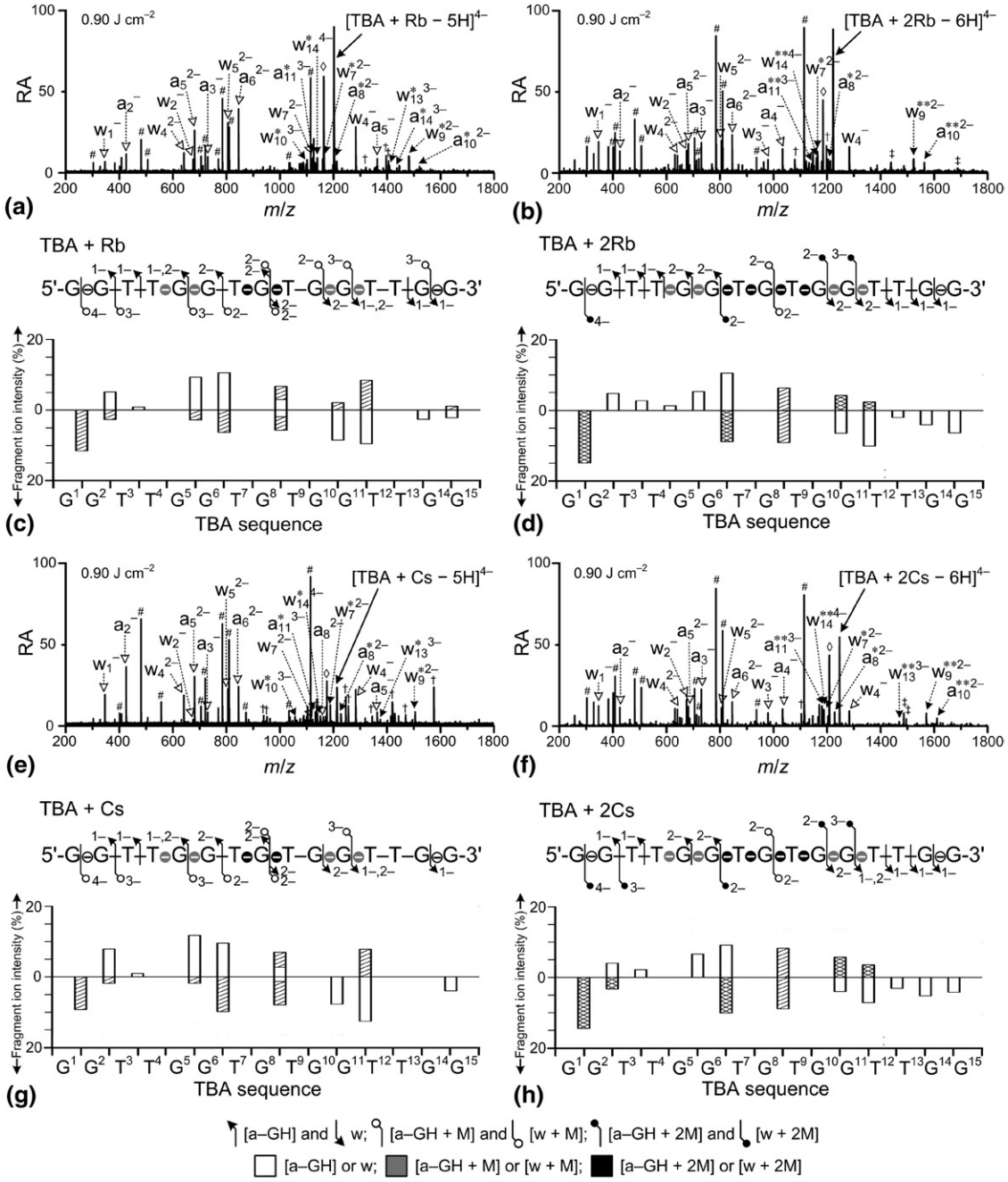

Figure 6. IRMPD spectra of (**a**) $[TBA + Rb^+ - 5H]^{4-}$ and (**b**) $[TBA + 2Rb^+ - 6H]^{4-}$ at 0.90 J cm^{-2}; fragmentation pattern, charge distribution and fragment ion intensity distribution from IRMPD of (**c**) $[TBA + Rb^+ - 5H]^{4-}$ and (**d**) $[TBA + 2Rb^+ - 6H]^{4-}$; IRMPD spectra of (**e**) $[TBA + Cs^+ - 5H]^{4-}$ and (**f**) $[TBA + 2Cs^+ - 6H]^{4-}$ at 0.90 J cm^{-2}; fragmentation pattern, charge distribution and fragment ion intensity distribution from IRMPD of (**g**) $[TBA + Cs^+ - 5H]^{4-}$ and (**h**) $[TBA + 2Cs^+ - 6H]^{4-}$.

Conclusions

The consecutive alkali metal binding constants on TBA are uniquely determined by ESI mass spectrometry. In addition, the binding sites of alkali metal ions on TBA are identified by IRMPD. The first potassium ion is coordinated between the bottom G-quartet and two adjacent TT loops of the G-quadruplex structure of TBA, while the second one is bound at the TGT loop. On the other hand, both the first and second alkali metal ions are bound at the GTGTG loop of TBA in the cases of sodium, rubidium, and cesium. The product of binding constants K_1 and K_2 for potassium is 5–8 times greater than those for other alkali metal ions. The adduct formation between the TGT loop and sodium, rubidium, cesium, or the second potassium ion is considered to be due to electrostatic interactions. Meanwhile, the first potassium ion appears to form a coordination complex between the two TT loops of TBA as

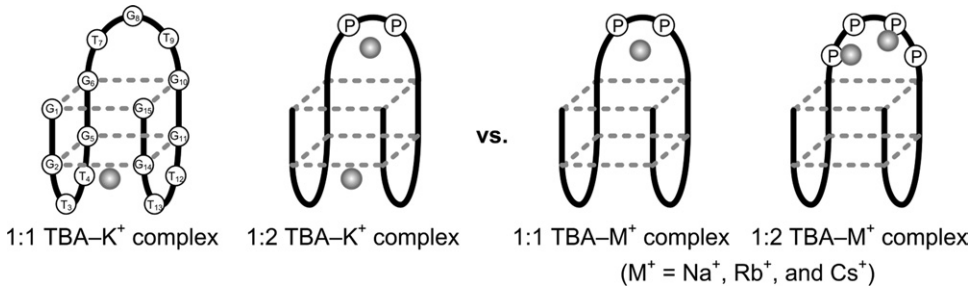

Scheme 1. Alkali metal binding sites of the G-quadruplex TBA. The first potassium ion is coordinated between the bottom G-quartet and two TT loops, and the second potassium ion bound at the distant TGT loop. Other alkali metals bind to the TGT loop sequentially up to two. All possible metal-binding phosphates are denoted by P in circle.

the fragment charge distribution suggests that four phosphate groups in the G^2–T^3–T^4 and T^{12}–T^{13}–G^{14} regions are not ionized.

Acknowledgments

The authors are thankful for the support from the Functional Proteomics Center (Grant FPR08A1-040) established by the Ministry of Education, Science, and Technology of the Republic of Korea. They gratefully acknowledge the Korea Research Institute of Standards and Science for access to the FT-ICR facility.

Appendix A
Supplementary Material

Supplementary material associated with this article may be found in the online version at doi:10.1016/j.jasms.2010.03.035.

References

1. Bock, L. C.; Griffin, L. C.; Latham, J. A.; Vermassa, E. H.; Toole, J. J. Selection of Single-Stranded DNA Molecules that Bind and Inhibit Human Thrombin. *Nature* **1992,** *355,* 564–564.
2. Macaya, R. F.; Schultze, P.; Smith, F. W.; Roe, J. W.; Feigon, J. Thrombin-Binding DNA Aptamer Forms a Unimolecular Quadruplex Structure in Solution. *Proc. Natl. Acad. Sci. U.S.A.* **1993,** *90,* 3745–3749.
3. Wang, K. Y.; McCurdy, S.; Shea, R. G.; Swaminathan, S.; Bolton, P. H. A DNA. Aptamer which Binds to and Inhibits Thrombin Exhibits a New Structural Motif for DNA. *Biochemistry* **1993,** *32,* 1899–1904.
4. Kelly, J. A.; Feigon, J.; Yeates, T. O. Reconciliation of the X-ray and NMR Structures of the Thrombin-Binding Aptamer d(GGTTGGTGTGGTTGG). *J. Mol. Biol.* **1996,** *256,* 417–422.
5. Padmanabhan, K.; Padmanabhan, K. P.; Ferrara, J. D.; Sadler, J. E.; Tulinsky, A. The Structure of α-Thrombin Inhibited by a 15-mer Single-Stranded DNA Aptamer. *J. Biol. Chem.* **1993,** *268,* 17651–17654.
6. Padmanabhan, K.; Tulinsky, A. An Ambiguous Structure of a DNA 15-mer Thrombin Complex. *Acta Cryst.* **1996,** *D52,* 272–282.
7. Hardin, C. C.; Watson, T.; Corregan, M.; Bailey, C. Cation-Dependent Transition between the Quadruplex and Watson-Crick Hairpin Forms of d(CGCG$_3$GCG). *Biochemistry* **1992,** *31,* 833–841.
8. Wong, A.; Wu, G. Selective Binding of Monovalent Cations to the Stacking G-Quartet Structure Formed by Guanosine 5′-Monophosphate: A Solid-State NMR Study. *J. Am. Chem. Soc.* **2003,** *125,* 13895–13905.
9. Siddiqui-Jain, A.; Grand, C. L.; Bearss, D. J.; Hurley, L. H. Direct Evidence for a G-quadruplex in a Promoter Region and its Targeting with a Small Molecule to Repress c-*MYC* Transcription. *Proc. Natl. Acad. Sci. U.S.A.* **2002,** *99,* 11593–11598.
10. Miyoshi, D.; Nakao, A.; Sugimoto, N. Structural Transition from Antiparallel to Parallel G-quadruplex of d($G_4T_4G_4$) Induced by Ca^{2+}. *Nucleic Acids. Res.* **2003,** *31,* 1156–1163.
11. Marathias, V. M.; Bolton, P. H. Determinants of DNA Quadruplex Structural Type: Sequence and Potassium Binding. *Biochemistry* **1999,** *38,* 4355–4362.
12. Kankia, B. I.; Marky, L. A. Folding of the Thrombin Aptamer into a G-quadruplex with Sr^{2+}: Stability, Heat, and Hydration. *J. Am. Chem. Soc.* **2001,** *123,* 10799–10804.
13. Vairamani, M.; Gross, M. L. G-Quadruplex Formation of Thrombin-Binding Aptamer Detected by Electrospray Ionization Mass Spectrometry. *J. Am. Chem. Soc.* **2003,** *125,* 42–43.
14. Loo, J. A. Electrospray Ionization Mass Spectrometry: A Technology for Studying Noncovalent Macromolecular Complexes. *Int. J. Mass Spectrom.* **2000,** *200,* 175–186.
15. Rosu, F.; De Pauw, E.; Gabelica, V. Electrospray Mass Spectrometry to Study Drug-Nucleic Acids Interactions. *Biochimie* **2008,** *90,* 1074–1087.
16. Wilson, J. J.; Brodbelt, J. S. Infrared Multiphoton Dissociation of Duplex DNA/Drug Complexes in a Quadrupole Ion Trap. *Anal. Chem.* **2007,** *79,* 2067–2077.
17. Mo, J.; Håkansson, K. Characterization of Nucleic Acid Higher Order Structure by High-Resolution Tandem Mass Spectrometry. *Anal. Bioanal. Chem.* **2006,** *386,* 675–681.
18. Gabelica, V.; Rosu, F.; De Pauw, E.; Lemaire, J.; Gillet, J.-C.; Poully, J.-C.; Lecomte, F.; Grégoire, G.; Schermann, J.-P.; Desfrançois, C. Infrared Signature of DNA G-quadruplexes in the Gas Phase. *J. Am. Chem. Soc.* **2008,** *130,* 1810–1811.
19. Sannes-Lowery, K. A.; Griffey, R. H.; Hofstadler, S. A. Measuring Dissociation Constants of RNA and Aminoglycoside Antibiotics by Electrospray Ionization Mass Spectrometry. *Anal. Biochem.* **2000,** *280,* 264–271.
20. Gabelica, V.; Galic, N.; Rosu, F.; Houssier, C.; De Pauw, E. Influence of Response Factors on Determining Equilibrium Association Constants of Non-covalent Complexes by Electrospray Ionization Mass Spectrometry. *J. Mass Spectrom.* **2003,** *38,* 491–501.
21. Zhang, S.; Van Pelt, C. K.; Wilson, D. B. Quantitative Determination of Noncovalent Binding Interactions Using Automated Nanoelectrospray Mass Spectrometry. *Anal. Chem.* **2003,** *75,* 3010–3018.
22. Wortmann, A.; Rossi, F.; Lelais, G.; Zenobi, R. Determination of Zinc to beta-Peptide Binding Constant with Electrospray Ionization Mass Spectrometry. *J. Mass Spectrom.* **2005,** *40,* 777–784.
23. Wilcox, J. M.; Rempel, D. L.; Gross, M. L. Method of Measuring Oligonucleotide–Metal Affinities: Interactions of the Thrombin Binding Aptamer with K^+ and Sr^{2+}. *Anal. Chem.* **2008,** *80,* 2365–2371.
24. Gabelica, V.; Rosu, F.; De Pauw, E. A Simple Method to Determine Electrospray Response Factors of Noncovalent Complexes. *Anal. Chem.* **2009,** *81,* 6708–6715.
25. Brodbelt, J. S.; Wilson, J. J. Infrared Multiphoton Dissociation in Quadrupole Ion Traps. *Mass Spectrom. Rev.* **2009,** *28,* 390–424.
26. Little, D. P.; Speir, J. P.; Senko, M. W.; O'Connor, P. B.; McLafferty, F. W. Infrared Multiphoton Dissociation of Large Multiply Charged Ions for Biomolecule Sequencing. *Anal. Chem.* **1994,** *66,* 2809–2815.
27. Little, D. P.; Aaserud, D. J.; Valaskovic, G. A.; McLafferty, F. W. Sequence Information from 42–108-mer DNAs (complete for a 50-mer) by Tandem Mass Spectrometry. *J. Am. Chem. Soc.* **1996,** *118,* 9352–9359.
28. Sannes-Lowery, K. A.; Hofstadler, S. A. Sequence Confirmation of Modified Oligonucleotides Using IRMPD in the External Ion Reservoir of an Electrospray Ionization Fourier Transform Ion Cyclotron Mass Spectrometer. *J. Am. Soc. Mass Spectrom.* **2003,** *14,* 825–833.
29. Keller, K. M.; Brodbelt, J. S. Collisionally-Activated Dissociation and Infrared Multiphoton Dissociation of Oligonucleotides in a Quadrupole Ion Trap. *Anal. Biochem.* **2004,** *326,* 200–210.
30. Yim, Y.-H.; Kim, B.; Ahn, S.; So, H.-Y.; Lee, S.; Oh, H. B. Evaluation of the Internal Temperature of an 8.6 kDa Protein Cation Exposed to a Hot Dispenser Cathode Employed in Electron Capture Dissociation Mass Spectrometry. *Rapid Commun. Mass Spectrom.* **2006,** *20,* 1918–1924.
31. Smirnov, I. V.; Shafer, R. H. Electrostatics Dominate Quadruplex Stability. *Biopolymers* **2007,** *85,* 91–101.
32. Vorlíčková, M.; Bednářová, K.; Kejnovská, I.; Kypr, J. Intramolecular and Intermolecular Guanine Quadruplexes of DNA in Aqueous Salt and Ethanol Solutions. *Biopolymers* **2007,** *86,* 1–10.

33. Katta, V.; Chait, B. T. Hydrogen/Deuterium Exchange Electrospray Ionization Mass Spectrometry: A Method for Probing Protein conformational Changes in Solution. *J. Am. Chem. Soc.* **1993,** *115,* 6317–6321.
34. Kaltashov, I. A.; Eyles, S. J. Studies of Biomolecular Conformations and Conformational Dynamics by Mass Spectrometry. *Mass Spectrom. Rev.* **2002,** *21,* 37–71.
35. Kumar, N.; Maiti, S. Quadruplex to Watson–Crick Duplex Transition of the Thrombin Binding Aptamer: A Fluorescence Resonance Energy Transfer Study. *Biochem. Biophys. Res. Commun.* **2004,** *319,* 759–767.
36. Nagatoishi, S.; Tanaka, Y.; Tsumoto, K. Circular Dichroism Spectra Demonstrate Formation of the Thrombin-Binding DNA Aptamer G-quadruplex under Stabilizing-Cation-Deficient Conditions. *Biochem. Biophys. Res. Commun.* **2007,** *352,* 812–817.
37. Marathias, V. M.; Bolton, P. H. Structures of the Potassium-Saturated, 2:1, and Intermediate, 1:1, Forms of a Quadruplex DNA. *Nucleic. Acids. Res.* **2000,** *28,* 1969–1977.
38. Jørgensen, T. J. D.; Roepstorff, P. Direct Determination of Solution Binding Constants for Noncovalent Complexes between Bacterial Cell Wall Peptide Analogues and Vancomycin Group Antibiotics by Electrospray Ionization Mass Spectrometry. *Anal. Chem.* **1998,** *70,* 4427–4432.
39. McLuckey, S. A.; Van Berkel, G. J.; Glish, G. L. Tandem Mass Spectrometry of Small, Multiply Charged Oligonucleotides. *J. Am. Soc. Mass Spectrom.* **1992,** *3,* 60–70.
40. Mao, X. A.; Gmeiner, W. H. NMR. Study of the Folding-Unfolding Mechanism for the Thrombin-Binding DNA Aptamer d(GGTTGGTGTGGTTGG). *Biophys. Chem.* **2005,** *113,* 155–160.